Precise location of the fault plane and the onset of the main rupture of the 2005 West Off Fukuoka Prefecture earthquake

Hiroshi Takenaka[1], Takeshi Nakamura[1], Yosuke Yamamoto[1], Genti Toyokuni[1], and Hiroshi Kawase[2]

[1]*Department of Earth and Planetary Sciences, Kyushu University, Hakozaki 6-10-1, Fukuoka 812-8581, Japan*
[2]*Department of Architecture and Urban Design, Faculty of Human-Environment Studies, Kyushu University, Hakozaki 6-10-1, Fukuoka 812-8581, Japan*

(Received August 11, 2005; Revised November 2, 2005; Accepted November 4, 2005; Online published January 27, 2006)

Near-source strong-motion records of the 2005 West Off Fukuoka Prefecture earthquake have two remarkable features. One is the presence of a relatively long period pulse with large amplitude on the fault-normal component of the velocity and displacement records, which is the result of the forward rupture directivity. The other is that the records show several seconds of small but increasing amplitude arrival ("initial rupture phase") followed by the onset of the main energy release ("main rupture phase"). We first determined the precise geometry of the fault plane of this earthquake by examining the horizontal particle motion of the main *S*-wave portion on the records, as follows: the strike is N304°E, and the dip angle is 87°. The dip direction of the fault plane is northeast, and the surface intersection of the fault plane passes by the eastern coast of Genkai Island. We also obtained the relative location of the onset of the main rupture with respect to the hypocenter, and the mean rupture velocity between them. The distance between them is 5.1 km, the onset of the main rupture is located southeast above the hypocenter. The mean rupture velocity along the straight path is 1.4 km/s. It is found that the main rupture began 3.6 sec later from the origin time, at the central point between the hypocenter and Genkai Island. Our results suggest that Genkai Island directly suffered the strong effects of the forward rupture directivity during the earthquake.

Key words: 2005 Fukuoka earthquake, fault plane, initial rupture, strong motion.

1. Introduction

The 2005 West Off Fukuoka Prefecture earthquake (M_{JMA}=7.0, hereafter called Fukuoka earthquake) occurred on 20 March 2005 (local time=UT+9 hours) in the northwestern offshore of Fukuoka Prefecture, Japan, which shook strongly Fukuoka city and surrounded area. No surface break associated with this earthquake fault was found. Aftershock distribution shows a northwest-southeast trend with about 30 km length (Fig. 1). Figure 2 and Table 1 show six reported focal mechanism solutions for the mainshock from NIED, ERI, JMA, Yamanaka (2005), USGS and Harvard. Assuming that a NW-SE nodal line of each focal mechanism corresponds to the fault plane, their features are as follows: the fault mechanism is almost pure left-lateral strike-slip; the strike is nearly parallel to N120°E or N300°E; the fault plane is almost vertical, and the dip direction is northeast (JMA and Yamanaka's solutions) or southwest (the others). We have examined the depth distribution of the aftershocks within 24 hours after the mainshock, and confirmed that the distribution is almost vertical, but it was difficult to find the dip direction from it.

During the mainshock in some part of Fukuoka city the JMA seismic intensity of 6− has been observed and many building damages were reported. In Genkai Island near the focal area, although no seismic intensity was measured for the mainshock, especially heavy damage of houses and landslides were reported.

Dense strong-motion observation networks were developed over Japan after the 1995 Kobe earthquake. In Fukuoka prefecture area, within the epicentral distance of 100 km, more than 120 strong-motion stations had been developed. Although no station was in the source region because this earthquake occurred in offshore, many strong-motion stations recorded the seismic motion near the source region. Figure 3(a) shows examples of such records. Stations P004 (Fukuoka Prefecture Seismic Intensity Network) and IF03 (FKOH03, KiK-net, NIED) are located in the vicinity of the southeast extension of the aftershock zone (see Fig. 1), and the epicentral distances are 31.1 km and 41.1 km, respectively. In the waveform at the two stations the following typical characteristics can be seen: first, remarkable impulsive motion of large amplitudes at the period of about 1–2 sec is present in crucial *S*-wave portion on the fault-normal (N30°E) component of velocity records, while the fault-parallel (N120°E) component motion is relatively small. Such a large amplitude pulse of relatively long period, so-called "killer pulse" is a near-fault effect, which is generated by the forward rupture directivity as also indicated from near-source records of several earthquakes (e.g., Heaton *et al.*, 1995; Somerville *et al.*, 1995; Kawase *et al.*, 2000).

The second feature is an emergent onset. The strong-

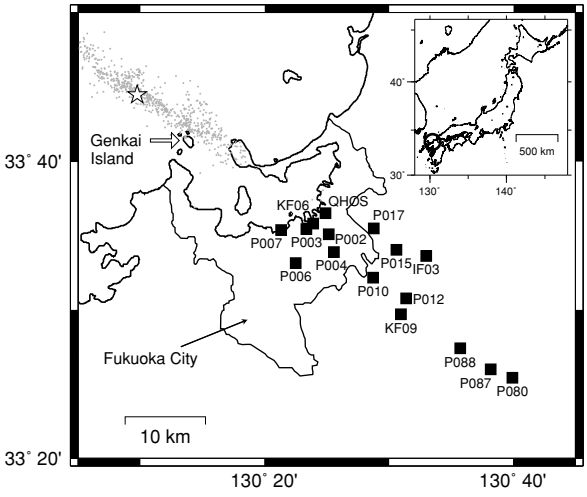

Fig. 1. The aftershock distribution within 24 hours after the mainshock, which was determined by SEVO, Kyushu University. The star indicates the epicenter of the mainshock. Squares depict the sixteen strong-motion stations whose mainshock records are used here for particle motion investigation. Station code: P*** are station no. *** of Fukuoka Prefecture Seismic Intensity Network, KF** are K-NET station FKO0** of NIED, IF** are KiK-net station FKOH** (GL) of NIED, QHOS is a station (GL) at Kyushu University Hospital. The gray dots are aftershocks. Five dots near station KF06 are events which occurred about 20 hours after the mainshock.

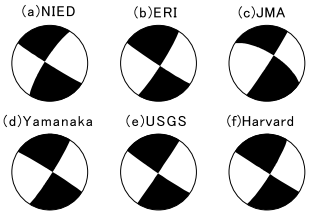

Fig. 2. Focal mechanism solutions of the mainshock obtained by (a) NIED (F-net, http://www.fnet.bosai.go.jp/freesia/event/tdmt/20050320015200/update1/index-j.html), (b) ERI (http://wwweic.eri.u-tokyo.ac.jp/topics/20050320/index-j.html#CMT), (c) JMA (http://www.seisvol.kishou.go.jp/eq/mech/outer/cmt/event/0503201053_.html), (d) Yamanaka (2005) (http://www.eri.u-tokyo.ac.jp/sanchu/Seismo_Note/2005/EIC163.html), (e) USGS (http://neic.usgs.gov/neis/eq_depot/2005/eq_050320/neic_vwac_q.html) and (f) Harvard CMT (http://neic.usgs.gov/neis/eq_depot/2005eq_050320/neic_vwac_hrv.html).

Table 1. Reported Solutions for the 2005 West Off Fukuoka Prefecture Earthquake.

Source	ϕ	δ	λ	M_w
(a) NIED	122°	87°	−11°	6.4
(b) ERI	123°	87°	6°	6.5
(c) JMA	302°	68°	−3°	6.7
(d) Yamanaka (2005)	302°	87°	−5°	6.6
(e) USGS	124°	87°	1°	6.5
(f) Harvard	122°	89°	8°	6.6

ϕ, δ, λ, and M_w are strike, dip, slip angle, and the moment magnitude, respectively.

motion records at local stations all show several seconds of small but increasing amplitude arrival (hereafter, called "initial rupture phase") followed by the onset of the main energy release (hereafter, called "main rupture phase"). Such an emergent onset is seen on teleseismic or strong-motion records of other earthquakes (e.g., the 1989 Loma Prieta earthquake: Wald *et al*., 1991; the 1992 Landers earthquake: Abercrombie and Mori, 1994; the 2000 Western Tottori earthquake, Hirata *et al*., 2002).

In Fig. 3(b), the initial rupture phase arrival and the main rupture phase arrival are denoted as P and P', respectively on the vertical component of velocity records. The hypocenter is determined by the first arrival, i.e. "P" time, so it corresponds to the rupture nucleation point. Difference between the arrival times of the initial and main rupture phases (hereafter, called $P'-P$ time) has information on the spatial relationship between the hypocenter and the onset location of the main energy release (main rupture).

In this letter, we determine the precise geometry (strike and dip angle) of the fault plane of this earthquake by examining the motion of the main S-wave portion on the near-source records, and then using $P'-P$ time at local strong-motion stations we derive the relative location of the onset of large energy release with respect to the hypocenter on the fault plane.

2. Determination of the Fault Plane

In order to determine the precise geometry of the fault plane, we adopt a procedure of Sekiguchi *et al*. (1996). They used a rotational characteristic of horizontal particle motion of each main S-wave pulse for locating the surface intersection of each fault segment for the 1995 Kobe earthquake. We examine the motion of the main S-wave portion including the "killer pulse" on the near-source strong-motion records of the Fukuoka earthquake at 16 stations located in the vicinity of the southeast extension of the aftershock zone (Fig. 1). Figure 4 shows displacement waveforms at stations shown in Fig. 1, except stations P004 and IF03 shown in Fig. 3.

Theoretically particle motion diagrams should show reverse rotation in the horizontal plane at the two stations located at the opposite sides of the surface intersection of the fault plane. When the rupture causes left-lateral faulting, particle motion is clockwise on the northeast side of the surface intersection, while counterclockwise on the southwest side, and the component perpendicular to the surface intersection is dominant, as schematically shown in Fig. 5. We compare this with the observed records. The observed motions of the main S-wave portion indicated by the bars in Fig. 4 are shown in Fig. 6. Particle motion at the 16 stations is of two types: at QHOS, P002, P015, P017 and IF03 (Group A) the rotation was clockwise; while at the other stations (Group B) it was counterclockwise.

The surface intersection of the fault plane should then locate southwest to Group A stations and northeast to Group B stations. In other words, the surface intersection line must be drawn so as to separate the two groups completely. We have drawn such a line manually, as shown in Fig. 6. The line has the azimuthal angle of 124° measured clockwise from the north, and it is an almost unique solution. If the azimuth of the line changed by more than one degree from 124°, the line could not separate Group A and B perfectly.

Note that the obtained surface intersection line is pass-

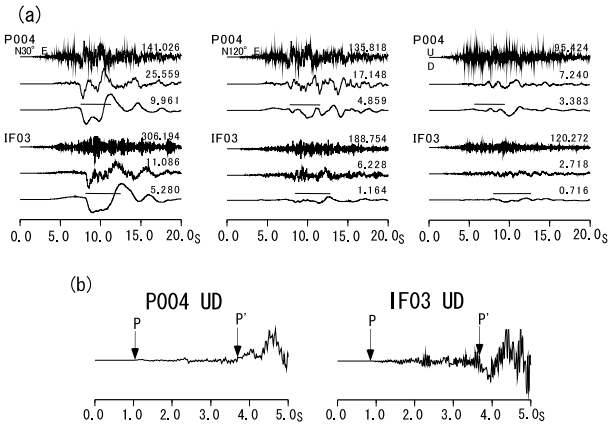

Fig. 3. (a) Examples of observed seismograms (acceleration, velocity and displacement from upper) in the vicinity of the southeast extension of the aftershock distribution trend. Left traces are the fault-normal (N30°E) component; middle traces the fault-parallel (N120°E) component; and right traces the vertical component. Maximum amplitude is at the end of each trace (acceleration: cm/s^2; velocity: cm/s; displacement: cm). Locations of stations P004 and IF03 are shown in Fig. 1. Bar above each waveform indicates the main *S*-wave portion. The horizontal particle motion diagrams of this portion are drawn in Fig. 6. (b) Zoomed waveform of vertical velocity.

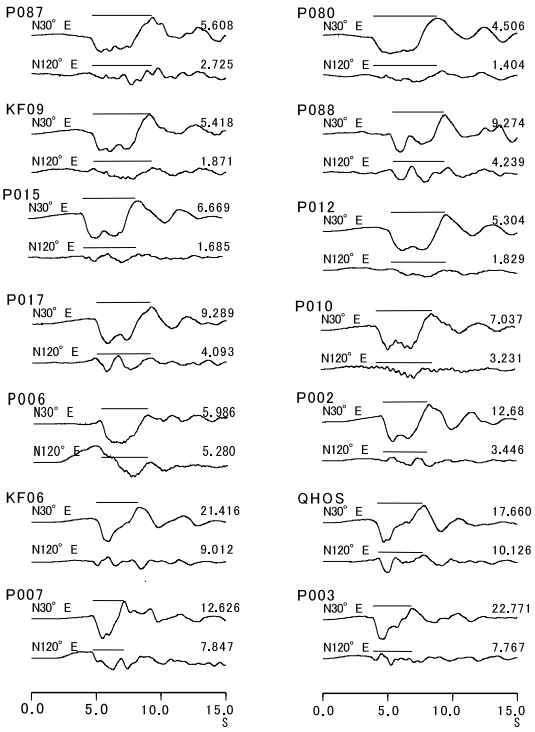

Fig. 4. Displacement waveforms observed at the stations shown in Fig. 1, except stations P004 and IF03 shown in Fig. 3. Upper traces are the fault-normal component (N30°E), and lower traces are the fault-parallel one (N120°E). Bar above each waveform indicates the main *S*-wave portion. The horizontal particle motion diagrams of this portion are drawn in Fig. 6.

ing just along the southwest edge of the aftershock zone. The fault plane can be constructed by this line and the hypocenter assuming that the hypocenter is located on the fault plane. Using point (lat. N33.7412°, long. E130.1623°, depth 9.89 km) as the hypocenter (Uehira *et al*., 2005), the dip direction and dip angle of the constructed plane are N34°E and 87°, respectively. The strike of the fault plane is then N304°E. To improve the hypocenter solution of the mainshock, Uehira *et al*. (2005) incorporated station corrections for *P*- and *S*-wave arrivals at the land-based seismic network which were determined using very accurate hypocenters and origin times of the aftershock events estimated from not only the land-based network data but also ocean bottom seismometers deployed over the aftershock zone and temporal stations installed at several small islands above and near the aftershock region. The estimated standard error for the mainshock epicenter is 0.31 km in the NS direction and 0.20 km in the EW direction, and for the depth is 0.75 km (Uehira, personal communication, 2005), which gives little dip angle change for the derived fault plane. The corresponding dip angle range is from 85° to 90°.

3. Location of the Main Rupture Onset

We now locate the main rupture starting point on the fault plane obtained in the previous section. Using $P' - P$ time at local strong-motion stations, we determine the relative location of the main rupture onset with respect to the hypocenter.

3.1 Method

We search the main rupture onset point over the fault plane. Figure 7 shows geometry of this problem. Let point S be the hypocenter, i.e. the initial rupture starting point, and S′ be the main rupture onset point. We assume that points S and S′ are both on the fault plane. We consider two-dimensional coordinate system ξ_1-ξ_2 in the fault plane, where the ξ_1-axis is set to be the strike of the fault, ξ_2-axis is taken positive updip, and the origin is taken at the hypocenter S.

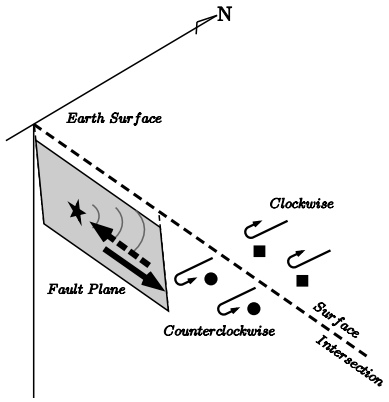

Fig. 5. Particle motion diagrams in the horizontal plane expected from a left-lateral strike-slip finite faulting. At stations indicated by a solid square, particle motion is clockwise, while at stations indicated by a solid circle, it is counterclockwise.

The arrival time difference between the initial rupture phase P and the main rupture phase P', $T_{P'-P}$ can then be represented as

$$T_{P'-P} = l\left(\frac{1}{v_r} - \frac{1}{v_p}\cos\Psi\right), \tag{1}$$

where l is the distance between points S and S′:

$$l = \sqrt{\xi_1^2 + \xi_2^2}. \tag{2}$$

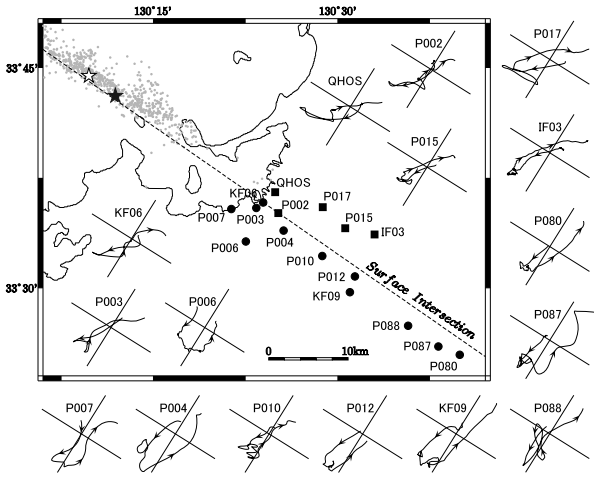

Fig. 6. Observed particle motion of the main S-wave portion. Each diagram is normalized by its maximum value. At stations indicated by a solid square particle motion was clockwise, while at stations indicated by a solid circle, it was counterclockwise. Broken line is the estimated surface intersection of the mainshock fault plane. The open star is the initial hypocenter, and the solid star indicates the location of the main rupture onset shown in Fig. 10(b).

Ψ is the angle between the vector $\overrightarrow{\mathrm{SS}'}$ and the ray direction of P wave at the hypocenter. $\cos\Psi$ is calculated as

$$\begin{aligned}\cos\Psi = \ & \sin i_\xi \cos(\phi-\phi_s)\cos\alpha \\ & -[\sin i_\xi \sin(\phi-\phi_s)\cos\delta \\ & \quad + \cos i_\xi \sin\delta]\sin\alpha,\end{aligned} \tag{3}$$

where i_ξ is the take-off angle of the ray measured from the depth direction, ϕ is the station azimuth, ϕ_s is the fault strike. α is measured counterclockwise in the fault plane as the angle between the vector $\overrightarrow{\mathrm{SS}'}$ and the ξ_1-axis, and

$$\cos\alpha = \xi_1/l, \quad \sin\alpha = \xi_2/l. \tag{4}$$

In Eq. (1) it has been assumed that the rays leaving S and S′ are parallel to each other.

Using measured data of $T_{P'-P}$ the onset location of the main rupture and rupture velocity are derived with a grid search method. In this inverse problem the unknown parameters to be searched are the ξ_1-, ξ_2-coordinates of S′ (or equivalently l and α) and the mean rupture velocity v_r along the path S to S′. This procedure minimizes the following:

$$\epsilon = \frac{1}{N}\sum_{j=1}^{N}[(T^O_{P'-P})_j - (T^C_{P'-P})_j]^2, \tag{5}$$

where N is the total number of stations, and $(T^O_{P'-P})_j$ and $(T^C_{P'-P})_j$ are the observational and the computational (predicted) time difference between P and P' arrivals at station j, respectively. $(T^C_{P'-P})_j$ are calculated using Eq. (1).

3.2 Data

We measured P and P' arrival time on the records at strong-motion stations whose epicentral distances are less than 43 km, where upgoing P waves emitted at the hypocenter arrives as the initial P phase. For 28 stations we could read clear onset time for both phases to measure the difference. Figure 8(a) shows the location of these 28 stations, and Fig. 8(b) plots the observed $P'-P$ time against the station azimuth. This plotting has a minimum around the direction of the surface intersection of the fault, which indicates that it is reasonable to assume that the main rupture starting point S′ is also located on the fault plane determined in the previous section.

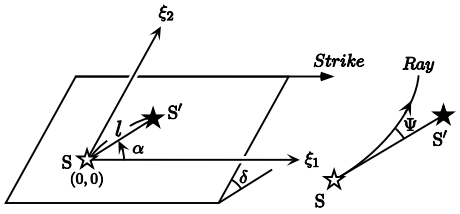

Fig. 7. Geometry for searching the main rupture onset point S′ over the fault plane. In the left panel, ξ_1-ξ_2 is a 2-D coordinate system in the fault plane. In the right panel, angle Ψ is defined as the angle between vector $\overrightarrow{\mathrm{SS}'}$ and the ray direction of P wave at the hypocenter S.

3.3 Results

We performed the grid search with the grid intervals for v_r, ξ_1 and ξ_2 of 0.1 km/s, 0.1 km and 0.1 km, respectively. The P-wave velocity around the hypocenter was assumed to be 6.0 km/s. It is the P-wave velocity at 10 km depth in the model for the aftershock determination by SEVO, Kyushu Univ. (Fig. 9), and also identical to the P-wave velocity of the upper crust assumed in a strong-motion prediction for Fukuoka city by Nakamichi and Kawase (2002). The take-off angle for each station was calculated using the P-wave velocity model shown in Fig. 9.

We show the results of the grid search in Fig. 10. The optimal values are $v_r = 1.4$ (km/s), $\xi_1 = -4.2$ (km), and $\xi_2 = 2.9$ (km), which give the mean squared residuals ϵ the minimum value of 3.5×10^{-3} (Figs. 10(a) and (b)). It corresponds to the rms residual time of 5.9×10^{-2} sec. In other words, with this accuracy, the relative location of S′ with respect to S has been determined. Figure 10(c) plots the data points around the predicted $T_{P'-P} - \cos\Psi$ line for the optimal v_r and position of S′. We can see that the most data points locate close to the line and show little scattering. It indicates that the derived v_r and location of S′ explain the observed $P'-P$ time data very well.

We here check the effects of the uncertainty of the velocity model on the solution by using a homogeneous structure model with the P-wave velocity of 6.0 km/s. The solution is then $v_r = 1.4$ (km/s), $\xi_1 = -4.3$ (km), and $\xi_2 = 2.6$ (km), which gives $\epsilon = 4.4 \times 10^{-3}$. This solution is almost identical to that for the velocity model shown in Fig. 9 although the residuals are larger. It is therefore concluded with enough accuracy that in this earthquake the main rupture began at a point of 5 km apart, southeast and up, from the hypocenter.

4. Discussion and Conclusions

In this paper we precisely located the surface intersection of the fault plane for the 2005 Fukuoka earthquake, and determined the fault strike and dip angle. The strike is N304°E, and the dip angle is 87°. The fault plane is thus nearly vertical with dip direction of northeast. We also ob-

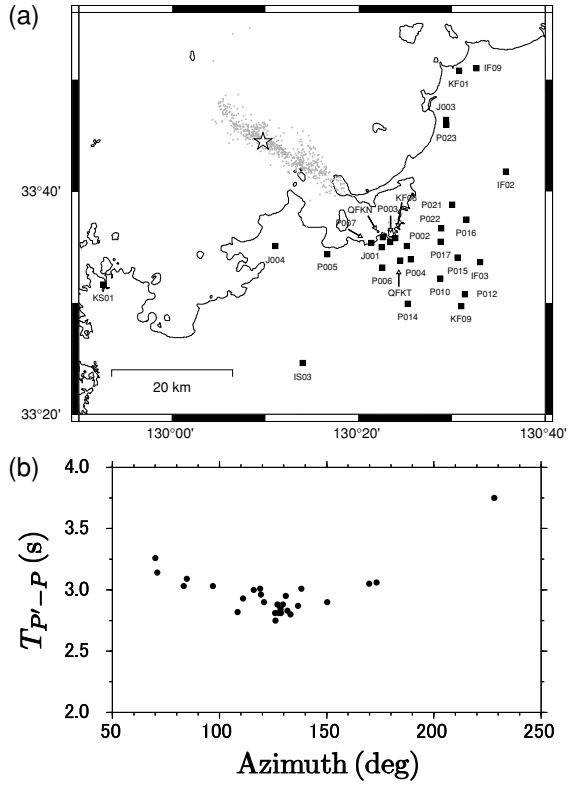

Fig. 8. (a) Map of the stations used for locating the main rupture onset. (b) Azimuthal dependence of the arrival time difference between the initial rupture phase P and the main rupture phase P', $T_{P'-P}$.

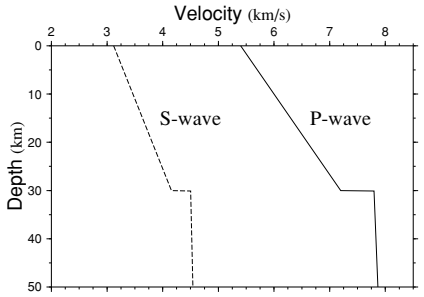

Fig. 9. Velocity structure model for the aftershock determination by SEVO, Kyushu University. The P-wave velocity model is used in calculation of the take-off angles for locating the main rupture onset.

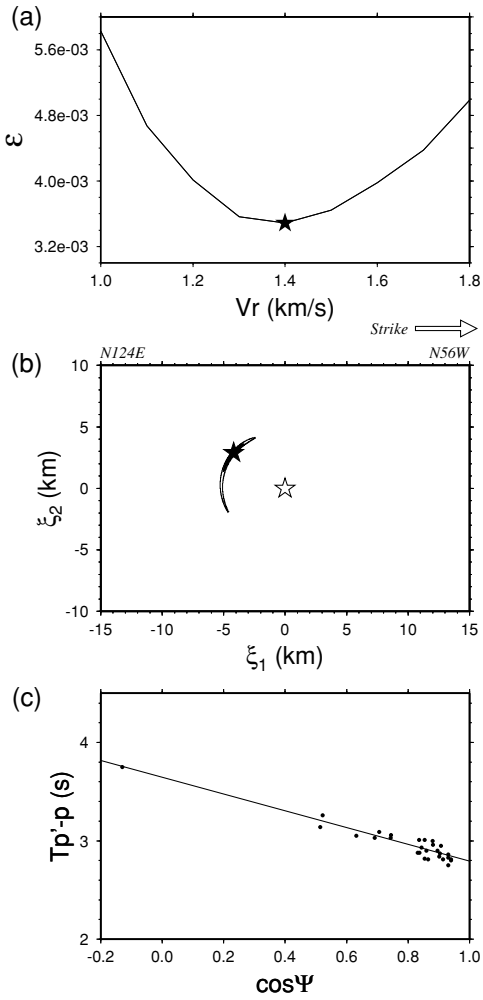

Fig. 10. Results of the grid search. (a) Plot of the minimum value of ϵ and the rupture velocity v_r. The optimal value of v_r is 1.4 km/s. (b) The contour map of the residual ϵ over the fault plane for $v_r = 1.4$ (km/s). Note that left is SE direction, while NW direction is right. The contours are shown for ϵ of less than 1.0×10^{-2}, which corresponds to the rms residual time of 0.1 sec, and the interval of contour is 5.0×10^{-3}. The position with the minimum value of ϵ is marked by a solid star. This position ($\xi_1 = -4.2$ (km), $\xi_2 = 2.9$ (km)) is the optimal location of the main rupture onset S′. The hypocenter S is also indicated by an open star. The distance between S and S′ (i.e. l) is then 5.1 km, and angle α is 145°. (c) Distribution of the data points around the $T_{P'-P} - \cos\Psi$ line for the optimal v_r and location of S′.

tained the relative location of the onset of the main rupture with respect to the hypocenter, and the mean rupture velocity between them. The distance between the two points is 5.1 km, and the onset of the main rupture is located southeast above the hypocenter. The mean rupture velocity along the straight path is 1.4 km/s, which indicates that the large energy release initiated 3.6 sec later from the origin time. This rupture velocity is 40% of the shear velocity at the depth of the rupture (see Fig. 9), which is much slower than the average rupture velocity (72%) of shallow crustal earthquake empirically obtained by Geller (1976). It might suggest a possibility that the initial rupture did not propagate directly from the hypocenter to the main rupture onset point along the straight path between them, but propagated along a curved path or stopped for a while between them. Although it is a very interesting subject, it may require a more advanced study to resolve it.

Several inverted source models have already been estimated from teleseismic or strong-motion data (e.g., Asano and Iwata, 2006; Yamanaka, 2005). Figure 11 shows the inverted source model from S-wave portion of the near-source strong-motion records by Asano and Iwata (2006). The strike and dip angle of the fault plane they assumed are N122°E and 87°, respectively. The region with relatively large slip, i.e. asperity, exists southeast above the hypocenter. Their inversion for the slip distribution from the S-wave portion of the records may be rather robust with respect to errors of the assumed fault geometry (strike and dip) and hypocenter position. Their fault plane is almost parallel to our derived one, and the relative locations to the hypocenter on the two planes are enough close to each other that our estimated location of the main rupture onset and

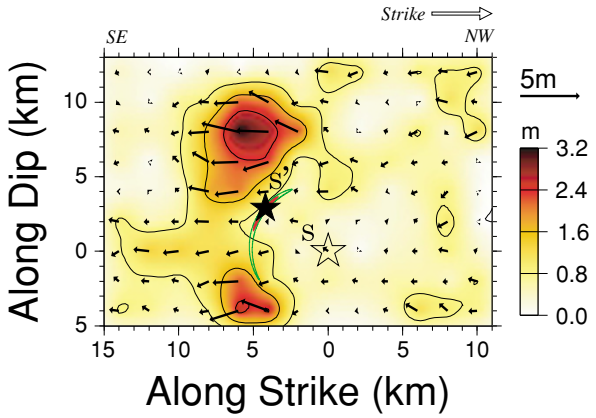

Fig. 11. Comparison of the main rupture onset derived here with Asano and Iwata's (2006) model of slip distribution. The main rupture onset point S′ and the estimated residual contours shown in Fig. 10(b) has been superimposed on their slip model. The contour interval of slip is 0.8 m (modified from Asano and Iwata, 2006).

the residual contours in Fig. 10(b) can be superimposed on their model matched with the hypocenter (Fig. 11). From Fig. 11, it is found that the main rupture onset point is located around bottom boundary of the asperity area southeast above the hypocenter, which may correspond to the starting point of the asperity break. The main rupture onset point was determined using *P*-wave portion of the strong-motion records, while Asano and Iwata's (2006) slip distribution was derived from *S*-wave portion of the records. Although both were estimated by using independent information, they show high consistency each other. From Fig. 11, it is expected that when the rupture nucleated at the hypocenter reached the bottom boundary of the asperity region, the main rupture, i.e. asperity slip, began at that point and the main energy was started to be released.

The surface intersection line of the fault plane obtained in Section 2 passes by the eastern coast of Genkai Island which had the most severe damage during this earthquake. The onset of the main energy release is located at just central point between the hypocenter and Genkai Island, as shown in Fig. 6 by the solid star. This spatial configuration suggests that the asperity began to break 3.6 sec after the origin time, from around the bottom of the asperity and the rupture front then swept the asperity upward and to the southeast, so that Genkai Island directly suffered the strong effects of the forward rupture directivity.

In this letter we have focused on the fault geometry and the spatial relationship between the hypocenter and the onset of the main rupture on the fault plane. The fault strike has been obtained only using the main *S*-wave portion of the strong-motion data with no assumption. Therefore strictly speaking it may be the strike of the main rupture (asperity) plane corresponding to the main *S*-wave portion. On the other hand, the fault dip estimation has been based on the assumption that the hypocenter and the main asperity share the same plane, which is usually employed for source inversion. As a result we obtained a fault plane which is very consistent with the focal mechanism solutions listed in Table 1. It may prove that this assumption is reasonable, at least in a macroscopic sense, to explain the strong ground motion. In a microscopic investigation on the physical process of the nucleation of the earthquake, it might be necessary to avoid use of this assumption. Such investigation is beyond the scope of this letter. It will be the near-future subject.

Acknowledgments. We used the strong-motion records supplied by Fukuoka Prefecture, the Japan Meteorological Agency (JMA) and the National Institute for Earth Science and Disaster Prevention (NIED; K-NET, KiK-net), and the hypocenter information determined by the Institute of Seismology and Volcanology (SEVO), Kyushu University. Mr. K. Uehira kindly provided us with the hypocenter information of the mainshock presented in the 2005 Japan Earth and Planetary Science Joint Meeting. The comments from Profs. J. Zahradnik and K. Yomogida, and an anonymous reviewer were helpful for improving the manuscript. We thank Mr. M. Ohshima who kindly helped parts of the data processing. Mr. K. Asano kindly provided us with their original figure for Fig. 11 in this letter. GMT (Wessel and Smith, 1991) was used for making several figures.

References

Abercrombie, R. and J. Mori, Local observations of the onset of a large earthquake, 28 June 1992 Landers, California, *Bull. Seism. Soc. Am.*, **84**, 725–734, 1994.

Asano, K. and T. Iwata, Source process and near-source ground motions of the 2005 West Off Fukuoka Prefecture earthquake, *Earth Planets Space*, **58**, this issue, 93–98, 2006.

Geller, R. J., Scaling relations for earthquake source parameters and magnitudes, *Bull. Seism. Soc. Am.*, **71**, 1501–1523, 1976.

Heaton, T. H., J. F. Hall, D. J. Wald, and M. W. Halling, Response of high-rise and base-isolated buildings to hypothetical M_W 7.0 blind thrust earthquake, *Science*, **267**, 206–211, 1995.

Hirata, M., Y. Umeda, and H. Kawakata, Initial rupture of the 2000 Western Tottori earthquake, *Chikyu Monthly, Spetial Issue*, **38**, 162–166, 2002 (in Japanese).

Kawase, H., S. Matsushima, R. W. Graves, and P. G. Somerville, Strong motion simulation of Hyogo-ken Nanbu (Kobe) earthquake considering both the heterogeneous rupture process and the 3-D basin structure, Proceedings of 12th World Conference on Earthquake Engineering, Auckland, New Zealand, CD-ROM Ref. No. 990, 8 pp., 2000.

Nakamichi, S. and H. Kawase, Broadband strong motion simulation in Fukuoka city based on a three-dimensional basin structure and a hybrid method, *J. Struct. Constr. Eng.*, AIJ, **560**, 83–91, 2002 (in Japanese with English abstract).

Sekiguchi, H., K. Irikura, T. Iwata, Y. Kakehi, and M. Hoshiba, Minute locating of faulting beneath Kobe and the waveform inversion of the source process during the 1995 Hyogo-ken Nanbu, Japan, earthquake using strong ground motion records, *J. Phys. Earth*, **44**, 473–487, 1996.

Somerville, P. G., N. F. Smith, R. W. Graves, and N. A. Abrahamson, Accounting for near-fault rupture directivity effects in the development of design ground motion, Proceedings of the 1995 ASME/JSME PVP Conference, Hawaii, July 23–27, 1995.

Uehira, K., M. Hori, H. Shimizu, T. Kanazawa, H. Miyamachi, M. Shinohara, Y. Iio, T. Okada, H. Takahashi, N. Kame, N. Matsuwo, T. Yamada, K. Nakahigashi, S. Hashimoto, K. Uchida, and M. Saito, Detailed aftershock activity by urgent joint seismic observation of the 2005 west off Fukuoka earthquake (M7.0), Abstr. Jpn. Earth Planet. Sci. Joint Meeting, X113-P005, 2005.

Wald, D. J., D. V. Helmberger, and T. H. Heaton, Rupture model of the 1989 Loma Prieta earthquake from the inversion of strong-motion and broadband teleseismic data, *Bull. Seism. Soc. Am.*, **81**, 1540–1572, 1991.

Wessel, P. and W. H. F. Smith, Free software helps map and display data, *EOS Trans. Am. Geophys. Union*, **72**, 441, 1991.

Yamanaka, Y., EIC seismological note: **163**, http://www.eri.u-tokyo.ac.jp/sanchu/Seismo_Note/2005/EIC163.html, 2005 (in Japanese).

H. Takenaka (e-mail: takenaka@geo.kyushu-u.ac.jp), T. Nakamura (e-mail: nakamura@geo.kyushu-u.ac.jp), Y. Yamamoto (e-mail: yosuke@geo.kyushu-u.ac.jp), G. Toyokuni (e-mail: toyokuni@geo.kyushu-u.ac.jp), and H. Kawase (e-mail: kawase@arch.kyushu-u.ac.jp).